Determination of chronological aging parameters in epidermal keratinocytes by *in vivo* harmonic generation microscopy

Yi-Hua Liao,[1,2,5] Szu-Yu Chen,[3,4] Sin-Yo Chou,[3] Pei-Hsun Wang,[3] Ming-Rung Tsai,[3] and Chi-Kuang Sun[2,3,*]

[1]*Department of Dermatology, National Taiwan University Hospital and College of Medicine, National Taiwan University, No.7, Chung-Shan South Road, Taipei 10002, Taiwan*
[2]*Molecular Imaging Center, National Taiwan University, No.1, Sec.4, Roosevelt Road, Taipei 10617, Taiwan*
[3]*Graduate Institute of Photonics and Optoelectronics and Department of Electrical Engineering, National Taiwan University, No.1, Sec.4, Roosevelt Road, Taipei 10617, Taiwan*
[4]*Graduate Institute of Optics and Photonics, National Central University, No.300, Jhongda Road, Jhongli City, Taoyuan 32001, Taiwan*
[5]*yihualiao@ntu.edu.tw*
*sun@ntu.edu.tw

Abstract: Skin aging is an important issue in geriatric and cosmetic dermatology. To quantitatively analyze changes in keratinocytes related to intrinsic aging, we exploited a 1230 nm-based *in vivo* harmonic generation microscopy, combining second- and third-harmonic generation modalities. 52 individuals (21 men and 31 women, age range 19–79) were examined on the sun-protected volar forearm. Through quantitative analysis by the standard algorithm provided, we found that the cellular and nuclear size of basal keratinocytes, but not that of granular cells, was significantly increased with advancing age. The cellular and nuclear areas, which have an increase of 0.51 μm^2 and 0.15 μm^2 per year, respectively, can serve as scoring indices for intrinsic skin aging.

© 2012 Optical Society of America

OCIS codes: (110.0180) Microscopy; (170.1530) Cell analysis; (170.1610) Clinical applications; (170.1870) Dermatology; (170.3880) Medical and biological imaging; (190.4160) Multiharmonic generation.

References and links

1. M. A. Farage, K. W. Miller, P. Elsner, and H. I. Maibach, "Intrinsic and extrinsic factors in skin ageing: a review," Int. J. Cosmet. Sci. **30**(2), 87–95 (2008).
2. K.-I. Nakamura, N. Izumiyama-Shimomura, M. Sawabe, T. Arai, Y. Aoyagi, M. Fujiwara, E. Tsuchiya, Y. Kobayashi, M. Kato, M. Oshimura, K. Sasajima, K. Nakachi, and K. Takubo, "Comparative analysis of telomere lengths and erosion with age in human epidermis and lingual epithelium," J. Invest. Dermatol. **119**(5), 1014–1019 (2002).
3. E. M. Buckingham and A. J. Klingelhutz, "The role of telomeres in the ageing of human skin," Exp. Dermatol. **20**(4), 297–302 (2011).
4. M. Sugimoto, R. Yamashita, and M. Ueda, "Telomere length of the skin in association with chronological aging and photoaging," J. Dermatol. Sci. **43**(1), 43–47 (2006).
5. S. I. S. Rattan, "Aging of skin cells in culture," in *Textbook of Aging Skin,* M. A. Farage, K. W. Miller, and H. I. Maibach, eds. (Springer-Verlag, Heidelberg, 2010), pp. 487–492.
6. N. A. Fenske and C. W. Lober, "Structural and functional changes of normal aging skin," J. Am. Acad. Dermatol. **15**(4), 571–585 (1986).
7. M. El-Domyati, S. Attia, F. Saleh, D. Brown, D. E. Birk, F. Gasparro, H. Ahmad, and J. Uitto, "Intrinsic aging vs. photoaging: a comparative histopathological, immunohistochemical, and ultrastructural study of skin," Exp. Dermatol. **11**(5), 398–405 (2002).
8. B. A. Gilchrest, "Skin aging and photoaging: an overview," J. Am. Acad. Dermatol. **21**(3), 610–613 (1989).
9. M. Gniadecka and G. B. Jemec, "Quantitative evaluation of chronological ageing and photoageing *in vivo*: studies on skin echogenicity and thickness," Br. J. Dermatol. **139**(5), 815–821 (1998).
10. J. M. Waller and H. I. Maibach, "Age and skin structure and function, a quantitative approach (I): blood flow, pH, thickness, and ultrasound echogenicity," Skin Res. Technol. **11**(4), 221–235 (2005).

11. S. Sakai, M. Yamanari, A. Miyazawa, M. Matsumoto, N. Nakagawa, T. Sugawara, K. Kawabata, T. Yatagai, and Y. Yasuno, "*In vivo* three-dimensional birefringence analysis shows collagen differences between young and old photo-aged human skin," J. Invest. Dermatol. **128**(7), 1641–1647 (2008).
12. S. Neerken, G. W. Lucassen, M. A. Bisschop, E. Lenderink, and T. A. Nuijs, "Characterization of age-related effects in human skin: A comparative study that applies confocal laser scanning microscopy and optical coherence tomography," J. Biomed. Opt. **9**(2), 274–281 (2004).
13. M. J. Koehler, K. König, P. Elsner, R. Bückle, and M. Kaatz, "*In vivo* assessment of human skin aging by multiphoton laser scanning tomography," Opt. Lett. **31**(19), 2879–2881 (2006).
14. M. J. Koehler, S. Hahn, A. Preller, P. Elsner, M. Ziemer, A. Bauer, K. König, R. Bückle, J. W. Fluhr, and M. Kaatz, "Morphological skin ageing criteria by multiphoton laser scanning tomography: non-invasive *in vivo* scoring of the dermal fibre network," Exp. Dermatol. **17**(6), 519–523 (2008).
15. C. Longo, A. Casari, F. Beretti, A. M. Cesinaro, and G. Pellacani, "Skin aging: *in vivo* microscopic assessment of epidermal and dermal changes by means of confocal microscopy," J. Am. Acad. Dermatol. (2011).
16. S.-Y. Chen, S.-U. Chen, H.-Y. Wu, W.-J. Lee, Y.-H. Liao, and C.-K. Sun, "*In vivo* virtual biopsy of human skin by using noninvasive higher harmonic generation microscopy," IEEE J. Sel. Top. Quantum Electron. **16**(3), 478–492 (2010).
17. S. Y. Chen, H. Y. Wu, and C.-K. Sun, "*In vivo* harmonic generation biopsy of human skin," J. Biomed. Opt. **14**(6), 060505 (2009).
18. T.-M. Liu, S.-W. Chu, C.-K. Sun, B.-L. Lin, P. C. Cheng, and I. Johnson, "Multiphoton confocal microscopy using a femtosecond Cr:forsterite laser," Scanning **23**(4), 249–254 (2001).
19. C. C. Wang, "Chromium-doped forsterite laser mode-locking and its applications," Graduate Institute of Photonics and Optoelectronics, Master Thesis (National Taiwan University, 1999).
20. M.-C. Chan, T.-M. Liu, S.-P. Tai, and C.-K. Sun, "Compact fiber-delivered Cr:forsterite laser for nonlinear light microscopy," J. Biomed. Opt. **10**(5), 054006 (2005).
21. T. Y. F. Tsang, "Optical third-harmonic generation at interfaces," Phys. Rev. A **52**(5), 4116–4125 (1995).
22. M. Müller, J. Squier, K. R. Wilson, and G. J. Brakenhoff, "3D microscopy of transparent objects using third-harmonic generation," J. Microsc. **191**(3), 266–274 (1998).
23. D. Débarre, W. Supatto, A.-M. Pena, A. Fabre, T. Tordjmann, L. Combettes, M.-C. Schanne-Klein, and E. Beaurepaire, "Imaging lipid bodies in cells and tissues using third-harmonic generation microscopy," Nat. Methods **3**(1), 47–53 (2006).
24. M. R. Tsai, S. Y. Chen, D. B. Shieh, P. J. Lou, and C.-K. Sun, "*In vivo* optical virtual biopsy of human oral mucosa with harmonic generation microscopy," Biomed. Opt. Express **2**(8), 2317–2328 (2011).
25. C. S. Hsieh, S. U. Chen, Y. W. Lee, Y. S. Yang, and C.-K. Sun, "Higher harmonic generation microscopy of *in vitro* cultured mammal oocytes and embryos," Opt. Express **16**(15), 11574–11588 (2008).
26. P. J. Matts, P. J. Dykes, and R. Marks, "The distribution of melanin in skin determined *in vivo*," Br. J. Dermatol. **156**(4), 620–628 (2007).
27. A. R. Haake, I. Roublevskaia, and M. Cooklis, "Apoptosis: a role in skin aging?" J. Investig. Dermatol. Symp. Proc. **3**(1), 28–35 (1998).
28. M. J. Koehler, S. Zimmermann, S. Springer, P. Elsner, K. König, and M. Kaatz, "Keratinocyte morphology of human skin evaluated by *in vivo* multiphoton laser tomography," Skin Res. Technol. **17**(4), 479–486 (2011).
29. G. Jenkins, "Molecular mechanisms of skin ageing," Mech. Ageing Dev. **123**(7), 801–810 (2002).
30. Y. Soroka, Z. Ma'or, Y. Leshem, L. Verochovsky, R. Neuman, F. M. Brégégère, and Y. Milner, "Aged keratinocyte phenotyping: morphology, biochemical markers and effects of Dead Sea minerals," Exp. Gerontol. **43**(10), 947–957 (2008).
31. Y. Barrandon and H. Green, "Cell size as a determinant of the clone-forming ability of human keratinocytes," Proc. Natl. Acad. Sci. U.S.A. **82**(16), 5390–5394 (1985).
32. M. Yaar and B. Gilchrest, "Aging of skin," in *Fitzpatrick's Dermatology in General Medicine,* I. M. Freedberg, A. Z. Eisen, K. Wolff, K. F. Austen, L. A. Goldsmith, and S. I. Katz, eds. (McGraw-Hill, New York, 2003), pp 1386–1398.
33. E. Brown, T. McKee, E. diTomaso, A. Pluen, B. Seed, Y. Boucher, and R. K. Jain, "Dynamic imaging of collagen and its modulation in tumors *in vivo* using second-harmonic generation," Nat. Med. **9**(6), 796–801 (2003).

1. Introduction

As an environmental barrier for human body, skin is affected by both intrinsic (chronological) and extrinsic aging [1]. While extrinsic aging is mainly caused by cumulative sunlight exposure, aging in non-exposed skin is attributed to inevitable intrinsic factors such as genetics and telomere length [2]. Accumulating evidence indicates that telomere shorting functions as a mitotic clock and leads to replicative senescence and skin aging [3,4]. In chronological aging, skin progressively becomes atrophic, dry, wrinkled, and often appears transparent and fragile [5]. Histologically, intrinsic aged skin is characterized by epidermal and dermal atrophy, increased heterogeneity in size of basal cells, flattening of the dermoepidermal junction, decreased vasculature, as well as reduced numbers of melanocytes, Langerhans cells and

fibroblasts [6,7]. These intrinsic aging-related changes result in increased vulnerability of skin as well as the disturbed skin barrier function, which caused increased incidence of inflammatory or infectious skin disorders in the elderly population [8]. Because geriatric health care has become a world-wide concern, an instrumental modality in examining and quantitatively defining the status of aging in skin cells is in demand.

Although histopathologic study is considered the gold standard technique to evaluate cellular morphologic changes for most dermatological diagnoses, the invasive nature of skin biopsy is not a suitable way to investigate skin aging in general populations. Instead, a noninvasive tool which is capable for revealing the cellular structure with high spatial resolution is more adaptive. Several *in vivo* noninvasive imaging methods with different image spatial resolution and measurable depth range, including ultrasound tomography [9,10], optical coherence tomography [11,12], multiphoton laser tomography [13,14], and reflectance confocal microscopy [15], have been exploited to investigate skin aging through different epidermal and dermal parameters. In our recent works, the 1230 nm-based higher harmonic generation microscopy, which combines second harmonic generation (SHG) and third harmonic generation (THG) modalities, has been successfully and safely used for noninvasive *in vivo* virtual optical biopsy on Asians' skin with a penetration depth of >300 μm [16,17]. Taking advantage of this technology advancement, we used this harmonic generation biopsy (HGB) system for *in vivo* study of skin aging. Because extrinsic skin aging is a multifactorial process related to different environmental factors and personal habits, we first invetigate the cellular morphological differences resulting from intrinsic aging. The goal of this study is primarily focused on the quantitative analysis of epidermal keratinocytes and to define morphological aging parameters resulting from chronological aging.

2. Materials and methods

2.1. Study population

Fifty-two Asians with 22 aged 19-29 years, 16 aged 30-59 years, and 14 aged above 59 years (21 men and 31 women, age range 19–79 years) of Fitzpatrick skin phototype III or IV were investigated. Measurements were performed at the ventral forearm about 15 cm proximal of the wrist. This study was conducted according to the Declaration of Helsinki Principles, and the protocol was approved by the Research Ethics Committee of National Taiwan University Hospital. Informed consent was obtained from each subject prior to study entry.

2.2. Cr:F-based HGB system

The HGB system as previously described was adapted from a commercial confocal scanning system (FV300, Olympus, Tokyo, Japan) combined with an inverted microscope (IX71, Olympus, Tokyo, Japan; Fig. 1(a)) [16]. A 1230 nm femtosecond Cr-F laser was used for excitation to lessen skin attenuation [18–20]. Using this system, a submicron and 1 μm resolution in lateral and axial directions and a >300 μm penetrability were achieved [16,17].

2.3. Skin-stabilization device

During the procedure of *in vivo* imaging, sample vibration due to breathing can lead to image blurring and reduce the spatial resolution. In this study, a vacuum-pump plate (Figs. 1(b) and 1(c)) was designed for sample stabilization. As shown in Fig. 1(b), the imaging window (IW) was in the middle and a circular intaglio (C) surrounding it was responsible for sucking the skin. Different from the syringe-pump adapter designed in a previous study [16], which sucked the skin within the IW, the vacuum-pump plate was designed to suck the skin surrounding the IW. A duct was drilled through the plate to connect the circular intaglio (C) to a vacuum pump. The skin could be stabilized when the vacuum pump started to pump out the air only in the circular intaglio (C). This vacuum-pump plate (Fig. 1(c)) was independent of the objective and could be translated in X- or Y-direction relative to the objective to achieve larger-area imaging. The
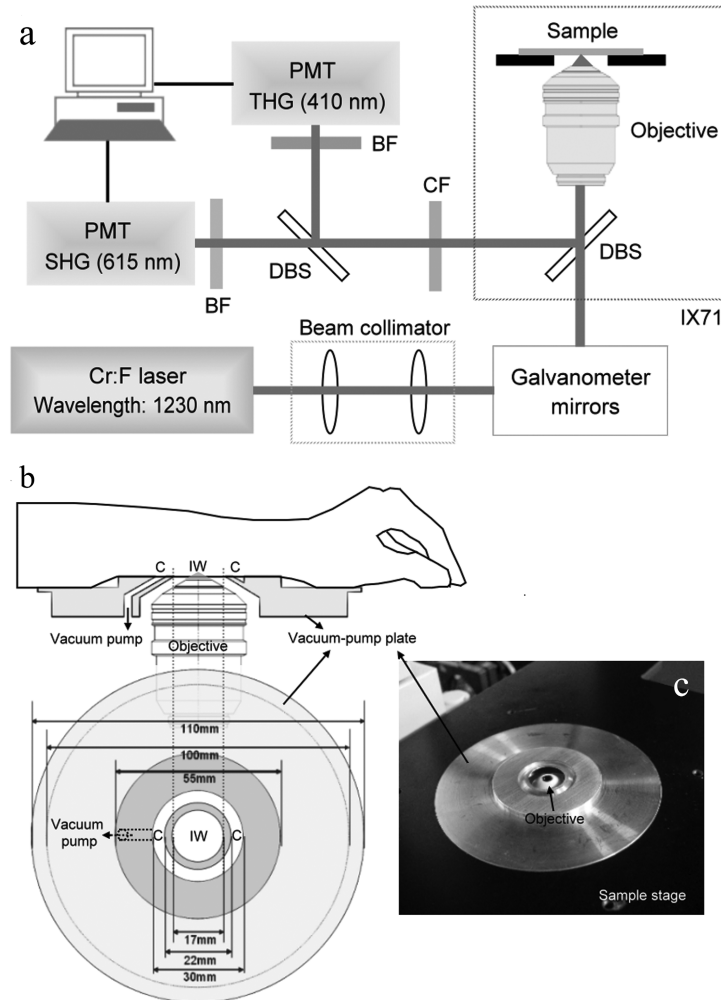
Fig. 1. (a) A schema of a 1230 nm-based HGB system adapted from a commercial confocal scanning system combined with an inverted microscope; DBS: dichroic beam splitter; CF: color filter; BF: band-pass filter; PMT: photomultiplier tube. (b) Sketch of a home-designed vacuum-pump plate used for sample stabilization; IW: imaging window; C: circular intaglio. (c) The implementation of the vacuum-pump plate which is combined with sample stage of inverted microscope.

vacuum-pump plate can also be adapted for various imaging angles. Besides, the imaging depth in the skin could be adjusted by moving the objective inside the IW with a motorized z-stage to perform 3-dimensional imaging. It is worth noticed that the IW of our suction head can be filled with water by sealing the IW with a circular cover glass and the water immersion objective, even the oil immersion objective, can be used.

2.4. Imaging protocols

In the HGB imaging, horizontal sections were obtained instead of vertical sections. By moving the objective in the z direction, stacks of image versus depth (XYZ) beginning from the stratum corneum, through the epidermis, and to the upper dermis were obtained for analysis. Five-μm step size was used. The image frame rate was 2.7 seconds per frame with 512×512 pixels. The image dimensions were approximately 120 μm × 120 μm.

2.5. Damage evaluation

For each volunteer, the total laser exposure time was limited to 30 minutes in the same area, and the average power measured right after objective was ~100 mW. Before and after the HGB, the test sites of all volunteers were recorded by photographing. In the early stage of this clinical trial, the tested sites of first 5 volunteers were evaluated by a dermatologist immediately, 1 hour, 24 hours, 3 days, and 1 week after HGB. The tested sites of next 47 volunteers were evaluated by a dermatologist immediately after HGB. After this two-stage damage evaluation, the rest of the volunteers were requested to contact us if they felt any discomfort during or after HGB. There were no cutaneous side effects such as erythema, pigment alteration, ulceration or blister formation. The procedure was comfortable and caused no itch or pain according to volunteers' opinions.

2.6. Analysis protocols

To reveal morphological features of granular and basal cells, analysis was performed on THG images obtained from the stratum granulosum and stratum basale. For the NC ratio analysis of basal cells and granular cells, at least 2 images (per volunteer) with the majority of cells sectioned were chosen. In each image, all the sectioned cells with nuclei were selected, and the total cytoplasmic and nuclear area was obtained by summing the individual cytoplasmic and nuclear area. The volumic NC ratio was obtained by dividing the total nuclear area by the total cytoplasmic area. For the analysis of the cellular and nuclear size of basal cells, at least 3 images (per volunteer) with the majority of basal cells with nuclei sectioned were chosen; in each image, the first 5-10 cells with the largest cross-section were selected for measuring the cell and nucleus areas and at least 25 cells were selected for each volunteer. For the analysis of the cellular and nuclear size of granular cells, at least 2 images (per volunteer) with the majority of granular cells sectioned were chosen; in each image, all cells were selected for measuring the cell and nucleus areas and at least 25 cells were selected for each volunteer. These criteria were to avoid measuring an off-centered cross-section area of the cell and the nucleus. These cellular parameters were evaluated by three independent observers.

2.7. Statistical analysis

The result of the cellular and nuclear size was expressed as mean ± standard deviation. The value of correlation coefficient between age and cellular/nuclear size was calculated using a Pearson linear regression model. One-way analysis of variance (ANOVA) or Kruskal-Wallis test was used for comparisons among three age groups. Statistics were performed with the SPSS 12.0 software (SPSS Inc., Chicago, IL), and $P < 0.05$ was considered statistically significant.

3. Results

3.1. In vivo HGB imaging of human skin

In vivo HGB imaging, including SHG and THG imaging, was performed on the volar forearm of 52 healthy Asian subjects. For each subject, a XYZ stack of HGB images was obtained from the stratum corneum to the upper dermis. As reported previously, the cellular morphology of the epidermis can be revealed through THG imaging, while the collagenous structures of the dermis can be shown by SHG signals [16,17]. As shown in Fig. 2(a), the THG contrast is much stronger in the stratum corneum than in other layers of the epidermis. This strong THG contrast is mainly contributed by the multilayer structures of the stratum corneum and lipids within the corneocytes [21–23]. In the viable cell layers of the epidermis, which includes the stratum granulosum (Fig. 2(b)), stratum spinosum (Fig. 2(c)), and stratum basale (Fig. 2(d)), the nuclei of the keratinocytes appeared dark under THG imaging, while the cytoplasm was observed THG-bright in contrast [24]. The THG signals in the cytoplasm are contributed by the cytoplasmic organelles [25]. With a strong imaging contrast between the nuclei and the cytoplasm, changes of the nuclear size, cellular size, and cell density can all be clearly revealed
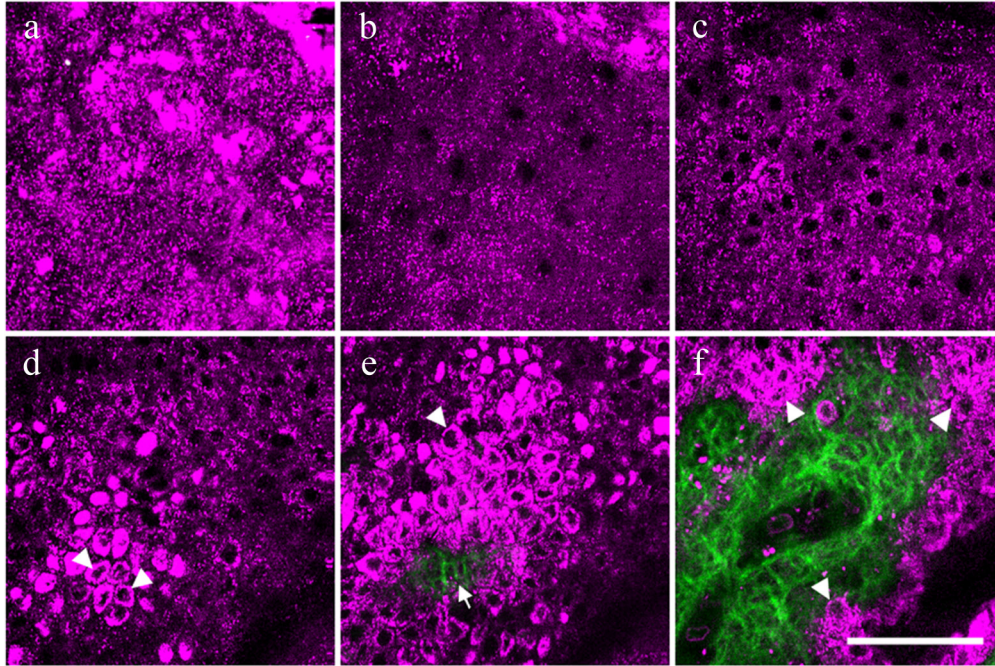
Fig. 2. A representative *in vivo* HGB image stack combining SHG and THG modalities from a 24-year-old Asian subject. The images were obtained from the volar forearm at different depths including the stratum corneum (a), the stratum granulosum (b), the stratum spinosum (c), and the stratum basale (d). At the stratum basale, the cytoplasm of the basal cells appeared THG-brighter (arrowheads) (d). At the dermoepidermal junction (e), collagen fibers were revealed by SHG (arrow), while the surrounding basal cells were shown by strong THG signals (arrowhead). As moving deeper inside papillary dermis (f), the borders of the basal cells (arrowheads) can also be clearly defined. THG and SHG are represented by magenta and green pseudo-colors, respectively. Scale bar = 50 μm.

in vivo. In the stratum basale, much brighter THG signals could be found in the cytoplasm (arrowheads in Fig. 2(d)). According to our previous study, the distribution of these brighter THG signals is correlated with the higher concentration of melanin in the basal cells [16,26]. Based on the enhanced THG contrasts, the THG-dark intercellular spaces between individual basal cells can be clearly resolved to precisely define cell borders. At an average depth around 100 μm, the epidermal rete ridges with a finger-like profile were observed. At the dermoepidermal junction (Fig. 2(e)), both the collagen fibers revealed by SHG (arrow in Fig. 2(e)) and the surrounding basal cells with strong THG contrasts (arrowhead in Fig. 2(e)) could be observed with the junction clearly defined. As moving deep to the papillary dermis, the area of the SHG-revealed dermal papillae begins to increase. The borders of the basal cells (arrowheads in Fig. 2(f)) can still be clearly defined with a sub-micron spatial resolution.

3.2. In vivo analysis of age-dependent alterations of granular cells

Aged skin is associated with thinning of epidermis, decreased proliferation, and increased apoptosis below the granular layer [27]. To gain insight into age-dependent alterations of keratinocytes, *in vivo* analysis based on THG imaging was performed to compare the difference between granular and basal cells. Figures 3(a)-3(d) show representative *in vivo* THG images obtained at the granular layer of forearm skin from four differently-aged volunteers (24, 47, 59, and 69 years old, respectively). Comparing the cellular morphology shown in these four images, no distinct differences related to age can be observed. Statistical analysis for cellular size, nuclear size, and nuclear-cytoplasmic ratio (NC ratio), was performed in 23 volunteers by the algorithm provided in Methods. We divided these 23 volunteers into three different-aged
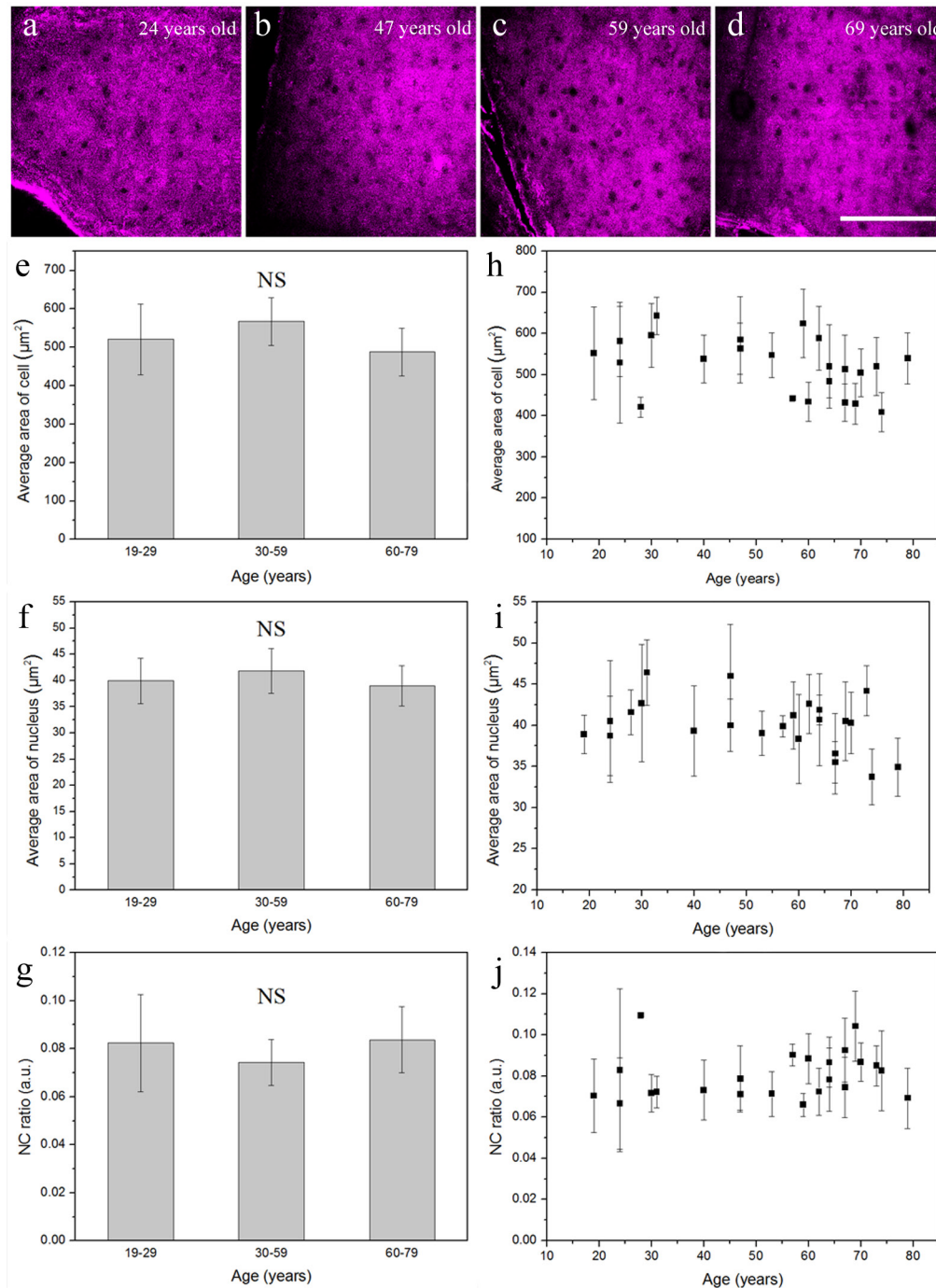
Fig. 3. Four representative *in vivo* THG images of epidermal granular cells obtained from the volar forearm of (a) 24-, (b) 47-, (c) 59-, and (d) 69-year-old volunteers. *In vivo* cytological analysis of (e) cellular size, (f) nuclear size, and (g) NC ratio of the granular cells showed no statistical difference between these three age groups. There was no significant correlation between (h) age and cellular size, (i) age and nuclear size, or (j) age and NC ratio. NS, no significance. Scale bar = 100 μm.

groups, 19-29, 30-59, and 60-79 years old. The average area of the granular cell was 520.7 ± 92.08 μm^2 at 19-29 years, 567.1 ± 51.66 μm^2 at 30-59 years, and 488.3 ± 62.04 μm^2 at 60-79 years (Fig. 3(e)). The average area of the nucleus was 39.9 ± 4.31 μm^2 at 19-29 years, 41.8 ± 4.27 μm^2 at 30-59 years, and 39.0 ± 3.84 μm^2 at 60-79 years (Fig. 3(f)). The NC ratio was 0.08 ± 0.020 at 19-29 years, 0.07 ± 0.010 at 30-59 years, and 0.08 ± 0.014 at 60-79 years (Fig. 3(g)). The cellular size, nuclear size, and NC ratio among these three different-aged groups showed no statistically significant difference (Table 1) (Kruskal-Wallis test; $P > 0.05$), and none of them was correlated with age (Figs. 3(h)-3(j)).

Table 1. Summary of the cellular area, nuclear area and N/C ratio of granular and basal cells observed by harmonic generation microscopy in three age groups

	Age group (years)			
	19-29	30-59	60-79	P value*
Stratum granulosum (n = 23)	n = 4	n = 8	n = 11	
Cellular area (μm^2)	520.7 ± 92.08	567.1 ± 51.66	488.3 ± 62.04	>0.05
Nucleus area (μm^2)	39.9 ± 4.31	41.8 ± 4.27	39.0 ± 3.84	>0.05
N/C ratio	0.08 ± 0.020	0.07 ± 0.010	0.08 ± 0.014	>0.05
Stratum basale (n = 52)	n = 22	n = 16	n = 14	
Cellular area (μm^2)	48.2 ± 3.98	60.2 ± 6.74	70.7 ± 6.47	<0.0001
Nucleus area (μm^2)	13.4 ± 1.72	15.8 ± 2.97	20.1 ± 2.79	<0.0001
N/C ratio	0.35 ± 0.022	0.35 ± 0.013	0.35 ± 0.016	>0.05

*P value is calculated by Kruskal-Wallis test (Stratum granulosum) or one-way ANOVA (stratum basale).
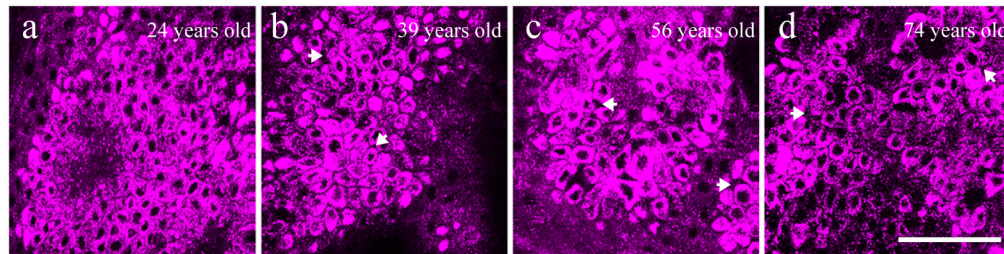

Fig. 4. Four representative *in vivo* THG images of epidermal basal cells obtained from the volar forearm of (a) 24-, (b) 39-, (c) 56-, and (d) 74-year-old volunteers. The widened THG-dark intercellular spaces between basal keratinocytes were indicated by arrows in (b-d). Scale bar = 50 μm.

3.3. In vivo analysis of age-dependent alterations of basal cells

Figure 4 showed representative *in vivo* THG images obtained at the basal layer of forearm skin from four differently-aged volunteers (24, 39, 56, and 74 years old, respectively). Comparing these four images, a more highly organized honeycomb structure of basal cells could be observed in the young skin (Fig. 4(a)), where the basal cells were in a regular oval shape. In contrast, basal cells in the older skin became irregular in shape and gradually lost the organized structures (Fig. 4(b)-(d)). In the stratum basale, the THG-dark intercellular spaces between basal keratinocytes in the aged skin (arrows in Fig. 4(b)-(d)) were wider and more irregular in width than those observed in the young group (Fig. 4(a)). It was found that the cellular and nuclear size seemed to be larger in the elderly comparing to the young subjects. In order to quantify these morphological observations, cytological analysis was performed on the THG images to reveal the correlation between the cellular/nuclear size and aging.

By using the algorithm given in Materials and methods, the cellular and nuclear size of the basal cells was analyzed from *in vivo* THG images of 52 healthy subjects, as revealed in Fig. 4. We found that the average area of the basal cell and its nucleus increased with advancing age. The average area of the basal cell was 48.2 ± 3.98 μm^2 at the age of 19-29 years, 60.2 ± 6.74 μm^2 at 30-59 years, and increased to 70.7 ± 6.47 μm^2 at 60-79 years (Fig. 5(a)). A strong positive
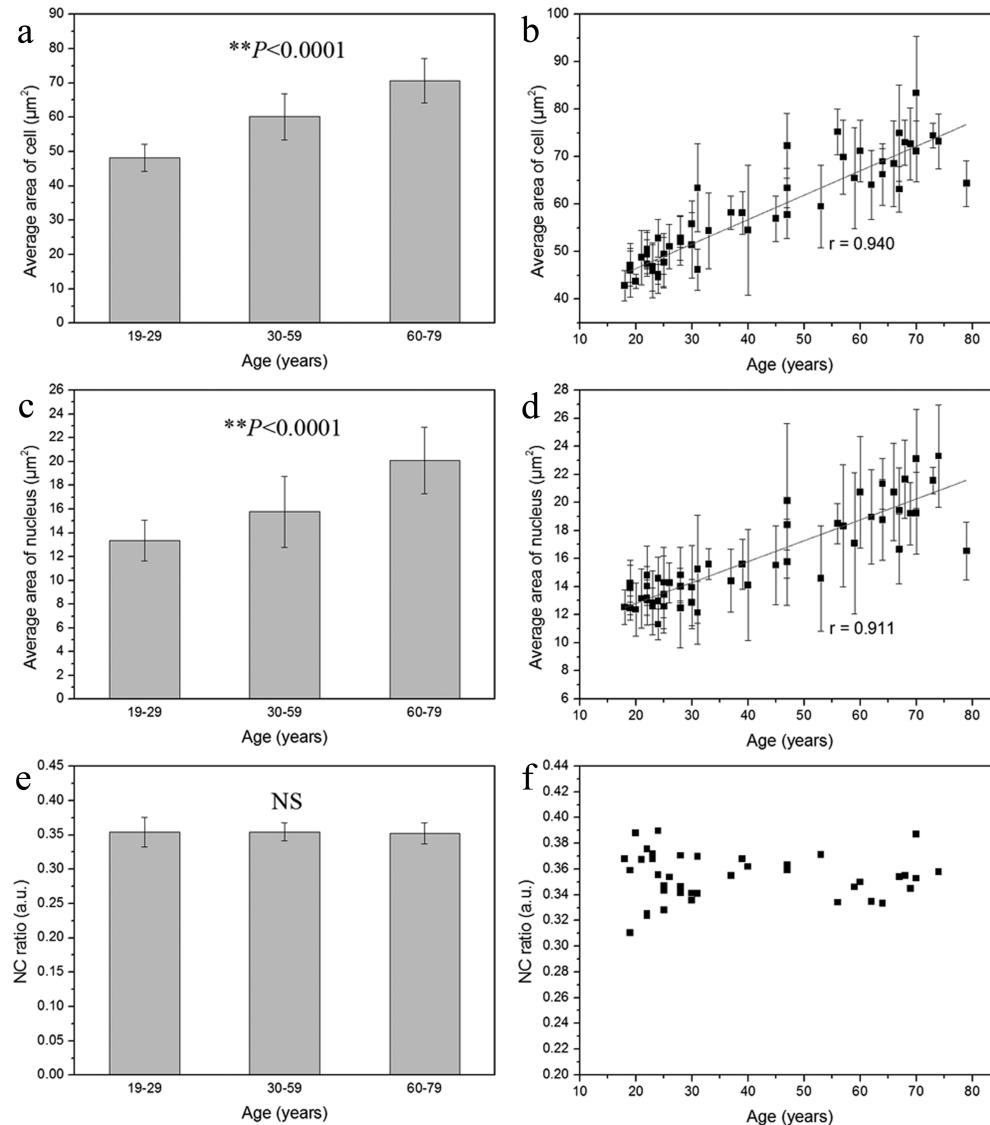
Fig. 5. The cellular size (a), nuclear size (c), and NC ratio (e) of the basal cells. A significant positive correlation was shown between age and the cellular area (b; correlation coefficient r = 0.940) as well as between age and the nuclear area (d; correlation coefficient r = 0.911) of basal cells; **$P < 0.0001$. No significant correlation was found between age and NC ratio (f); NS, no significance.

correlation was observed between the cellular size and age (Fig. 5(b); Pearson correlation coefficient r = 0.940). On the other hand, as shown in Fig. 5(c), the average area of the nucleus was 13.4 ± 1.72 μm^2 at the age of 19-29 years, 15.8 ± 2.97 μm^2 at 30-59 years, and increased to 20.1 ± 2.79 μm^2 at 60-79 years. A strong positive correlation was also observed between the nuclear size and age (Fig. 5(d); r = 0.911). Based on the linear regression equations, the average area of cell = $36.18 + 0.51 \times$ age and the average area of nucleus = $9.82 + 0.15 \times$ age, indicating that the cellular area increased 0.51 μm^2 and the nuclear area increased 0.15 μm^2 per year. The one-way ANOVA analysis also showed a statistically significant difference in the cellular and nuclear size among these three different-aged groups (Figs. 5(a) and 5(c); $P < 0.0001$). Besides, greater standard deviation of the cellular and nuclear size was found in subjects over 30 years

old (Figs. 5(a) and 5(c), vertical bars), which suggested that the basal cells and their nuclei became polymorphic and increased in heterogeneity with advancing age.

In addition to the analysis of the cellular and nuclear size, the volumic NC ratio of the basal cells from each subject was analyzed. From Fig. 5(e), it was found that the NC ratio remained consistent among different-aged groups. The NC ratio of basal cell was 0.35 ± 0.022 at the age of 19-29 years, 0.35 ± 0.013 at 30-59 years, and 0.35 ± 0.016 at 60-79 years, as shown in Fig. 5(f). The average NC ratio of basal cells from all the subjects was 0.35 ± 0.018. Comparing among these three different-aged groups, there was no statistically significant age-dependent difference in the NC ratio of basal cells (one-way ANOVA; $P > 0.05$). The cellular size, nuclear size, and NC ratio of basal keratinocytes among these three different-aged groups were summarized in Table 1. Taken altogether, we found that the cellular and nuclear size of basal keratinocytes, but not that of granular cells, was significantly increased with advancing age.

Moreover, we found that there were no significant gender differences in the cellular and nuclear size of the basal cells (Student's t-test; $P > 0.05$, respectively). The average area of the basal cell was 57.3 ± 10.97 μm^2 in women and 58.9 ± 10.59 μm^2 in men. The average area of the nucleus was 15.7 ± 3.18 μm^2 in women and 16.2 ± 3.39 μm^2 in men. In addition, according to the linear regression analysis, strong positive correlations were observed between the cellular size and age in female (Fig. 6(a); Pearson correlation coefficient r = 0.923) and male subjects (Fig. 6(b); r = 0.956), respectively. A statistically significant linear relationship was also found between the nuclear size and age in both female (Fig. 6(c); r = 0.883) and male subjects (Fig. 6(d); r = 0.924). The above results showed that the positive correlation of cellular/nuclear size of basal keratinocytes and age did not differ by gender.
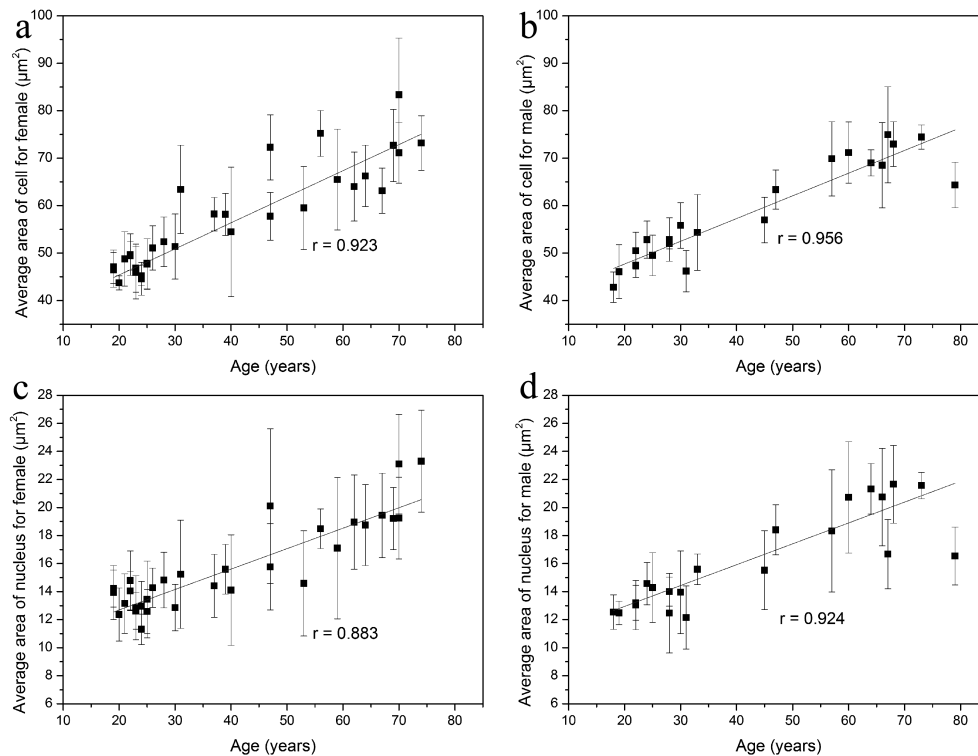

Fig. 6. The cellular (a, b) and nuclear size (c, d) of the basal cells in female and male subjects. A significant positive correlation was shown between age and the cellular area as well as between age and the nuclear area in female (a and c) and male subjects (b and d). r, correlation coefficient.

4. Discussion and conclusion

From the *in vivo* virtually biopsied images of the granular and basal layers, we analyzed if there was any age-related changes in nuclear area, cytoplasmic area, and NC ratio of sun-protected skin. We demonstrated that the cellular size, nuclear size, and NC ratio of granular cells showed no statistically significant differences among three different-aged groups. These results coincided with the recent study based on multi-photon fluorescence technique, where Koehler *et al.* found that the areas of the keratinocytes and their nuclei remained constant in the stratum granulosum in different age groups [28]. However, we found that in the stratum basale, both the cellular and nuclear areas enlarged with advancing age. Besides, the variability of individual cell and nucleus in the basal layer as shown by the standard deviations increased in the age groups beyond 30 years. The age-dependent increase of the epidermal basal cellular and nuclear size agrees with the proposed mechanism of keratinocyte senescence [5]. Senescence, which represents a state of G1 cell cycle arrest without division during serial passages, was proposed to be an underlying cause of aging. In the epidermis, it was reported that intrinsic aging is accompanied by replicative senescence of the keratinocytes and a progressive decline of clonogenic and proliferative cells below the granular layer [29]. In agreement with our results, previous *in vitro* cell culture studies have shown that keratinocyte senescence associated with intrinsic aging displayed increase in cell size [30]. Cellular size was known as a major determinant of the keratinocytes clonogenic ability that declines with intrinsic aging [31]. The enlarged cellular and nuclear size in aged basal cells could result from accumulation of intracellular debris such as lipofusin, formation of autophagic vacuoles, or multinucleation due to impaired cytokinesis [31]. In summary, the strong positive correlation between cellular and nuclear size and advancing age is found to be a unique phenomenon in the stratum basale in our study. Therefore, the cellular or nuclear size of the basal keratinocytes could act as a significant index for determining intrinsic skin aging.

The small deviation of the NC ratio for each volunteer indicated a good consistency of the analysis protocol based on THG imaging. According to our results, the NC ratio remained consistent in differently-aged skin. Koehler *et al.* also showed no difference of the NC ratio between different age groups [28]. However, when malignant transformation like actinic keratoses occurred, we observed that the NC ratio of keratinocyte became significantly higher comparing to normal skin [16,28].

We also observed that some intercellular spaces between individual basal cell became widened as skin aged. Similar findings of widened inter-keratinocyte spaces have been found in sun-protected skin in some extent through electron microscopy analysis [32]. This THG-revealed change of the intercellular spaces implies that the connection between the basal cells becomes looser and would contribute to the fragility of aged skin. Further studies are required to clarify this observatory phenomenon.

This study involves the application of *in vivo* HGB to investigate morphological changes of keratinocytes associated with intrinsic skin aging. Compared to the multiphoton fluorescence technique, SHG and THG leave almost no energy in the interacted matters and possess the noninvasiveness nature [33]. From this research, the cellular and nuclear size of basal keratinocytes is found to be good indices for scoring intrinsic skin aging. Take advantage of its histologic resolution to analyze cellular size, nuclear size as well as NC ratios in epidermal keratinocytes, HGB is applicable to identify actinic keratosis, Bowen's disease, squamous cell carcinoma, and basal cell carcinoma. Combining the noninvasive nature, high resolution, high penetration, safety and the three-dimensional sectioning power of THG microscopy, *in vivo* HGB is expected to become a new methodology in future dermatological clinical diagnosis, serial evaluation of treatment, and cosmetic research.

Acknowledgments